PRECISION MEASUREMENT MEETS ULTRAFAST CONTROL*

J. YE, S. BLATT, M. M. BOYD, S. M. FOREMAN, T. IDO, R. J. JONES, A. D. LUDLOW, A. MARIAN, K. MOLL, M. NOTCUTT, M. STOWE, M. THORPE, AND T. ZELEVINSKY

JILA, National Institute of Standards and Technology and Univ. of Colorado and Department of Physics, University of Colorado Boulder, Colorado 80309-0440, USA
E-mail: Ye@jila.colorado.edu

Optical spectroscopy and frequency metrology at the highest level of precision and resolution are being greatly facilitated by the use of ultracold atoms and phase stabilized light in the form of both cw and ultrashort pulses. It is now possible to pursue simultaneously coherent control of quantum dynamics in the time domain and high precision measurements of global atomic structure in the frequency domain. These coherent light-based precision measurement capabilities may be extended to the XUV spectral region, where new possibilities and challenges lie for precise tests of fundamental physical principles.

1. Introduction

Recent developments in atomic, molecular, and optical physics have been in the frontier of coherent manipulation of both matter and light fields. Indeed, ultracold atoms that exhibit macroscopic quantum properties are one of the exciting areas of research for the quest of an ultimate assembly and control of the microscopic or even the mesoscopic world. In parallel, capabilities in the generation and control of coherent light fields, including the generation of coherent optical bandwidth across the entire visible spectrum with spectral phase control and the maintenance of spectacularly long optical phase coherence time, permit the the full revelation of the quantum nature of light-matter interactions. In particular, the combination of ultracold atoms and phase-controlled ultra-wide-bandwidth optical frequency combs has had a profound impact to precision measurement science. In

*This work is supported by ONR, AFOSR, NSF, NASA, and NIST

this contribution we will present some of the recent results in JILA on precision spectroscopy of ultracold atoms using femtosecond combs and discuss the possibility of extending these scientific endeavors to the EUV region by producing precise comb structure there via extreme nonlinear optics.

Ultracold strontium atoms provide exciting opportunities to explore precision spectroscopy, quantum optics, and next generation optical atomic clocks.[1,2] In our laboratory we have explored a variety of ideas and measurement techniques for the strontium clock transitions, including free space spectroscopy of the 7.5kHz $^1S_0$ - $^3P_1$ transition in ultacold bosonic ^{88}Sr,[3] optical lattice based spectroscopy of the sub-Hz hyperfine induced $^1S_0$ - $^3P_0$ transition in fermionic ^{87}Sr,[4] and indirect spectroscopy of the strictly forbidden $^1S_0$ - $^3P_0$ transition in ^{88}Sr using an electromagnetically-induced-transparency (EIT) resonance.[5] A precisely stabilized optical frequency comb now enables Hz-wide laser linewidths[6] to be measured and controlled across optical frequency gaps and linked to the microwave primary standard, permitting precise and accurate spectroscopy of narrow linewidth transitions of Sr atoms loaded in an optical lattice. This capability of phase coherently linking cw lasers with wavelength separations of hundreds of nanometers will be very valuable for the proposed EIT scheme that relies on tight optical Raman coherence to realize the strictly scalar optical clock transition in ^{88}Sr.[5]

With precise control of both time- and frequency-domain properties of a pulse train, we have combined these two applications in a spectroscopic study of ultracold Rb atoms, achieving united time-frequency spectroscopy for structure and dynamics.[7,8] The work demonstrates precision spectroscopy of global atomic structure by a direct use of a single, phase-stabilized femtosecond optical comb. Furthermore, the pulsed nature of excitation allows real-time monitoring and control capabilities for both optical and quantum coherent interactions and state transfer. It is a synthesis of the fields of precision spectroscopy and coherent control: While at short time scales we can monitor and control the coherent accumulation and population transfer, at long times scales we recover all the information pertinent to the atomic level structure at a resolution limited only by the atomic natural linewidth under a spectral coverage spanning hundreds of terahertz. The combination of frequency domain precision and time domain dynamics represents a powerful approach for spectroscopy.

To extend the coherent frequency comb structure and related precision measurement capabilities into the deep UV spectral region, we have recently demonstrated high-harmonic generation (HHG) at 100 MHz repetition rates

enabled by a femtosecond enhancement cavity.[9,10] HHG provides a coherent source of vacuum-ultraviolet to soft x-ray radiation and it has traditionally relied on high-energy, low repetition rate amplified laser systems to provide the peak intensities needed for ionization of the gas target. The small conversion efficiency of the process, combined with the low repetition rate of amplified laser systems, results in low average powers of the generated XUV source. Furthermore, the use of these sources as precision spectroscopic tools[11,12] is limited, as the original laser frequency comb structure is lost in the HHG process. Using a femtosecond laser coupled to a passive optical cavity, coherent frequency combs in the XUV spectral region are generated via high-harmonics of the laser without any active amplification or decimation of the repetition frequency. We can thus significantly improve the average power conversion efficiency and reduce the system cost and size, while dramatically improving the spectral resolution. The presence of the frequency comb structure in the XUV and its extreme spectral resolution will enable similar revolutions in precision measurement, quantum control, and ultrafast science as in the visible region.

2. Precision spectroscopy and optical clock of Sr

Large ensembles of ultracold alkaline earth atoms have provided impressive short-term clock stability.[13,14] So far, interrogation of neutral atom based optical standards has been carried out primarily in free space, unavoidably including atomic motional effects that typically limit the overall system accuracy.[13,14,3] A promising approach is to explore the ultranarrow optical transitions of atoms held in an optical lattice.[15,16,17] The atoms are tightly localized so that Doppler and photon-recoil related effects on the transition frequency are eliminated.[18] Meanwhile, the trapping potential is created at a carefully chosen laser wavelength ($\lambda_{\rm magic}$) such that it has essentially no effect on the internal clock transition frequency.[19,20] Additionally, the increased atom-probe laser interaction time enabled by the lattice confinement will permit a full utilization of the narrow natural linewidth. This optical lattice approach using neutral atoms may provide the best possible combination of clock stability and accuracy. Such a proposal has been under intensive investigation in the case of the doubly forbidden $^1S_0$ - $^3P_0$ transition in the fermionic Sr isotope, ^{87}Sr.[21,15] Similar work in Yb is also in progress.[22,23]

The first high precision absolute frequency measurement was recently reported for the ^{87}Sr $^1S_0$ - $^3P_0$ clock transition using a GPS-based frequency

reference.[15] With a direct reference to the NIST F1 Cs fountain clock, here we report with the smallest statistical uncertainty to date the JILA measurement of this ultranarrow clock transition in a magic wavelength optical lattice. We have investigated systematic frequency shifts including those originating from atomic density, wavelength and intensity of the optical lattice, residual magnetic field, and probing laser intensity.

Figure 1 summarizes the measurement of the $^1S_0$ - $^3P_0$ transition frequency within three months. The statistical uncertainty of these measurements is 2.8 Hz. The most basic systematic error associated with spectroscopy in an optical lattice is the AC Stark shift of the clock transition due to the confining optical potential. To experimentally determine the magnitude and uncertainty of this shift, we vary the lattice intensity around the typical operating intensity of $I_0 = 35$ kW/cm^2 at wavelengths below, above, and near $\lambda_{\rm magic}$. At the typical operating wavelength of 813.437 nm, Fig. 1(a) shows the frequency shift as a function of intensity. The slope of this shift yields an overall correction of 17(8.3) Hz at the typical lattice intensity of I_0. We have also experimentally determined that for the lattice intensity of I_0, the induced frequency shift is $\sim$2 mHz for a lattice frequency deviation of 1 MHz from the magic wavelength. Combining this with our measurement of the lattice AC stark shift of 17 Hz at 813.437 nm yields $\lambda_{\rm magic} = 813.418(10)$ nm, in agreement with Ref. 15.

With potentially high atomic densities in an optical lattice, characterization of density shifts is important. We have $\sim$400 lattice sites with typically $\sim$250 atoms per site, yielding densities of $\sim 10^{12}$ atoms/cm^3. Varying the atomic density by a factor of 50 (Fig. 1(b)), we find the density shift at our typical operating density of 2×10^{12} atoms/cm^3 to be 2(13) Hz. Asymmetric population distributions among $^1S_0$ ground state m_F sublevels can lead to Zeeman shifts of the transition frequency. We measure a shift of 32 Hz/G (Fig. 1(c)). By keeping the magnetic field $<$400 mG during spectroscopy, the Zeeman shift uncertainty is 12 Hz. The probe beam itself can induce a frequency shift through two different physical mechanisms. The first is the AC Stark shift of the $^1S_0$ and $^3P_0$ levels due to their couplings to other states by the probe laser. For our investigation, the AC Stark shift due to the probe laser is exacerbated by using an electro-optic (EO) modulator to probe the atoms with a weak sideband while retaining an off resonant carrier for use in our fiber noise cancellation signal. The second frequency shift mechanism arises from the possibility of a small probe beam misalignment with respect to the lattice laser, permitting photon recoil shifts in the transverse direction of the optical trap. We separate these power-

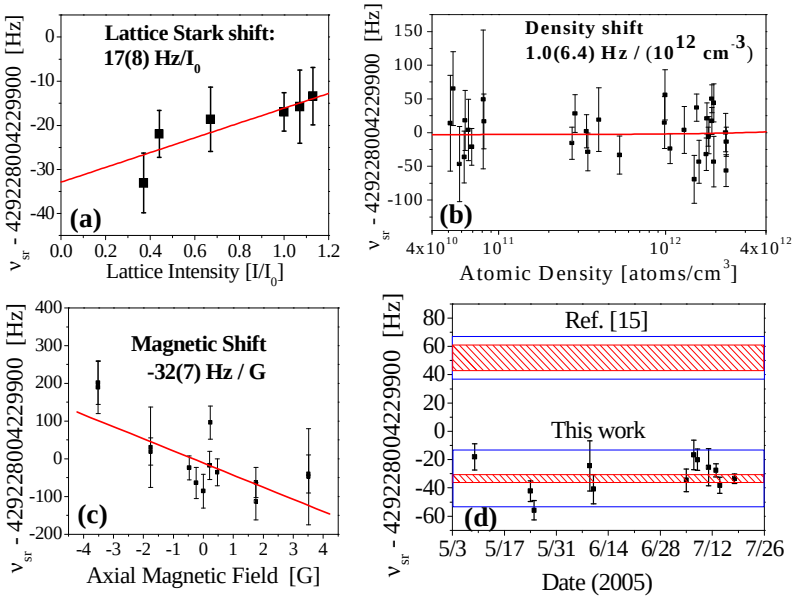

Figure 1. The measured ^{87}Sr $^1S_0$ - $^3P_0$ transition frequency versus (a) lattice intensity ($I_0 = 35$ kW/cm^2), (b) atomic density, and (c) magnetic field. (d) JILA measurements over a 3 month period, with each data point representing an averaged daily frequency measurement. The results reported in this work (lower bars) and in Ref. 15 (upper bars) are both shown with the total (outer box) and statistical (inner shaded area) errors.

dependent effects by either varying the total 698 nm light intensity incident on the atoms or changing the relative carrier-sideband amplitude through the EO modulation index. We determine each of these effects within 2 Hz uncertainty.

The frequency reference used for the optical measurement is a hydrogen maser directly calibrated by the NIST F1 Cs fountain clock, available to us by an optical fiber link from NIST to JILA.[24] The approximate 14 m lower elevation of our JILA Sr experiment relative to the NIST fountain clock introduced a < 1 Hz gravitational shift. Including all systematic effects discussed here and others with much smaller magnitudes, the total uncertainty (added in quadrature) is 20 Hz. The final number we report for the ^{87}Sr $^1S_0$ - $^3P_0$ transition frequency is 429, 228, 004, 229, 867 $\pm$ 20(sys) $\pm$ 2.8(stat) Hz. We note this result disagrees by three standard deviations with that of Ref. 15 measured with a GPS-calibrated reference.[4]

3. United Time Frequency Spectroscopy

Recent work has demonstrated that an optical frequency comb is a highly efficient tool for precise studies of atomic structure.[7,8] A phase-stabilized femtosecond comb has been used as an effective tool to perform direct spectroscopy of one- and two-photon transitions in ultracold Rb atoms, permitting high-resolution spectroscopy of all atomic transitions anywhere within the comb bandwidth. By measuring the previously unmeasured absolute frequency of the $5S_{1/2} \rightarrow 7S_{1/2}$ two-photon transitions in ^{87}Rb, we show that prior knowledge of atomic transition frequencies is not essential for this technique to work, and indicate that it can be applied in a broad context. Additionally, this approach enables precise studies of time domain dynamics, coherent accumulation and interference, and quantum control.[7]

In this contribution we discuss only one particular aspect of direct frequency comb spectroscopy (DFCS), namely coherent accumulation and population transfer effects in multilevel systems probed by multiple comb components. The importance of understanding these dynamics for precision spectroscopy is highlighted by the measurement of the 5P states. The $5S_{1/2} \rightarrow 5P_{1/2,3/2}$ transitions are probed both directly via one-photon DFCS (Fig. 2(a) left panel) and indirectly via two-photon DFCS of the 5S-5D two-photon transition that enjoys resonant enhancement when comb components are scanned through the intermediate 5P states (Fig. 2(a) right panel). Comparison between these two approaches clearly demonstrate the importance of including the dynamic population changes arising from pulse-accumulated population transfer in this indirect measurement.

A density-matrix based theoretical model describing the interaction of the femtosecond comb with atoms accounts for detailed dynamics of population transfer among the atomic states involved in transitions within the comb bandwidth. Impulsive optical excitation followed by free evolution and decay is used to model the interaction with each pulse in the train. The density matrix equations are solved to a fourth order perturbative expansion in the electric field and an iterative numerical scheme is employed to obtain the state of the atomic system after an arbitrary number of pulses.[25,7] This model is applied to accurately predict the coherent population accumulation in the relatively long-lived 5D or 7S states, followed by incoherent optical pumping. Especially important for the indirect 5P measurements is the incoherent optical pumping to the ground state hyperfine levels, which depends critically on the 5P state detunings.

The one-photon DFCS employs a single optical comb component and

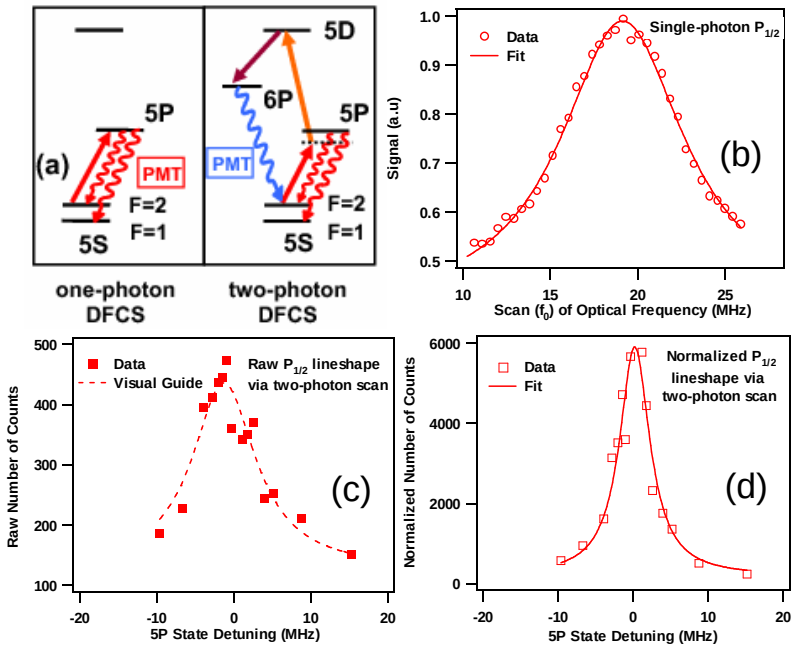

Figure 2. (a) Schematic of one- and two-photon DFCS, used for measuring single-photon transition frequencies. (b) Lineshape of the $5S_{1/2}$ F=2 $\rightarrow$ $5P_{1/2}$ F'=2 transition obtained from a scan of f_o for a fixed value of f_r, by one-photon DFCS. (c) Raw counts for the same lineshape as in (b) by two-photon DFCS, along with a visual guide for the data. (d) Normalized lineshape corresponding to the raw data in (c), obtained by using results from theory simulations accounting for optical pumping effects.

makes radiative detections directly from the 5P states (Fig. 2(a) left panel). Frequency scans are carried out by stepping continuously the carrier-envelope offset frequency f_o while keeping the repetition frequency f_r fixed at a convenient value. This one-photon transition lineshape is shown in Fig. 2(b). The absolute optical frequency of the $5S_{1/2}$ F=2 $\rightarrow$ $5P_{1/2}$ F'=2 transition in the D_1 manifold is determined.[8] For the corresponding two-photon DFCS experiment we map the $5S_{1/2}$ F=2 $\rightarrow$ $5P_{1/2}$ F'=2 $\rightarrow$ $5D_{3/2}$ F"=3 two-photon transition. we use a set of different pairs of f_r and f_o specifically chosen to have varying detunings from the 5P state for each data point shown in Fig. 2(c), while at the same time satisfying the 5S-5D two-photon resonance. The lineshape in Fig. 2(c) is retrieved by detecting the 420 nm fluorescence signal originating from 5D as a function of 5P state detuning produced by these (f_r, f_o) pair selections, along with

a visual guide for the data. The apparent linewidth is significantly broader than that associated with the 5P state. The pairs of f_r and f_o used to obtain each point in Fig. 2(c) lead to substantially different detunings of the other 5P states and subsequently, varying optical pumping to the F=1 ground state. Indeed, the theory model applied to the actual experiment conditions predicts significantly different ground state population transfer dynamics. The asymptotic values of the F=2 ground-state population are not the same for symmetric detunings from the intermediate state. Figure 2(d) presents the Lorentzian lineshape resulting from the normalization of the raw data shown in Fig. 2(c) with respect to theoretical values of the ground state population. After implementing this normalization, the transition lineshape resumes the same linewidth as shown in Fig. 2(b) and the transition frequency measured by the two-photon DFCS agrees with the corresponding one-photon DFCS result within the error bar.[8]

4. XUV frequency comb

Using a femtosecond laser coupled to a passive optical cavity, we can now address some of the issues associated with traditional high harmonic generation, namely average power, system size and cost, and spectral resolution. We demonstrate coherent frequency combs in the XUV spectral region from the generation of high-harmonics of the laser without any active amplification or decimation of the repetition frequency. The output from the laser is stabilized to a femtosecond enhancement cavity with a gas jet at the intracavity focus. The high-peak power of the intracavity pulse enables efficient HHG (Fig. 3). Since little of the fundamental pulse energy is converted, a fs enhancement cavity is ideally suited for HHG as the driving pulse is continually "recycled" after each pass through the gas target. HHG at high repetition rates opens the door for dramatic improvements in average power conversion efficiency. In addition, system cost and size are greatly simplified. Optical-heterodyne-based measurements reveal that the coherent frequency comb structure of the original laser is fully preserved in the high-harmonic generation process. These results lead the way for precision frequency metrology at extreme wavelengths and permit efficient HHG using only a standard laser oscillator.

To sufficiently build up the intracavity pulse energy, the passive optical cavity needs to incorporate a number of important characteristics: i) a high finesse,[26] ii) low round-trip group-delay dispersion to allow ultrashort pulses to be coupled into and stored inside the cavity,[27] and iii) a robust servo to

stabilize the two degrees of freedom of the incident pulse train to the corresponding cavity resonance modes.[28] A standard modelocked femtosecond Ti:Sapphire laser with 100 MHz f_r, 60-fs pulse duration, and 8 nJ pulse energy is used. The pulse train from the laser passes through a prism-based compressor before incident on the passive optical cavity. To investigate the peak intensity that can be obtained with this method, an empty fs enhancement cavity is initially characterized. With the laser locked to the cavity, the transmitted spectrum shows the effect of the residual cavity dispersion limiting the intracavity pulse bandwidth. Measurement of the transmitted pulse verifies that the pulse is nearly Fourier-transform-limited with a duration of 60 fs. The duration of the pulse is minimized inside the cavity by adjusting the compressor while measuring the current produced from a plasma in Xe at the focus. The intracavity pulse energy is enhanced up to 4.8 μJ for these short pulses, approximately a 600-fold increase from the incident pulse energy of 8 nJ. Based on these measurements we estimate a peak intracavity intensity of $> 3 \times 10^{13}$ W/cm^2 is obtained at the intracavity focus.

To couple the HHG light out of the cavity, a 0.7 mm-thick sapphire plate is placed at Brewster's angle (for the IR) inside the cavity. The Fresnel reflection coefficient of the intracavity plate rises at shorter wavelengths, with a reflectivity of 5-10% between 40 and 100 nm. The gas target is confined within a thin, hollow brass cylinder, with a 150 μm hole to allow the intracavity pulse to pass through (Fig. 3). The diffracted pattern of the HHG light, obtained with a MgF_2-coated aluminum grating, demonstrates that at least the 9th order harmonic has so far been generated. The average power of the 3rd harmonic light generated inside the cavity reaches nearly 10 μW. The corresponding intracavity single-shot efficiency ($\sim 10^{-8}$) is comparable to traditional femtosecond-amplifier-based systems at similar intensity levels. This demonstrates the dramatic increase in high-harmonic power that can be accessed using a high repetition rate (100 MHz). Clearly there is significant potential to further improve this efficiency and produce harmonics far into the XUV simply by increasing the incident pulse energy, easily allowing access to intensities $> 10^{14}$ W/cm^2 at high repetition rates.

In order to utilize the precision of the fs comb in the XUV spectral region, it must be verified that no detrimental phase/frequency fluctuations in the high-harmonic generation process exist. To test this we allow the original comb to drive two independent nonlinear processes, one through well characterized bound electronic nonlinearities based on second harmonic and sum frequency generation via two BBO optical crystals and the other

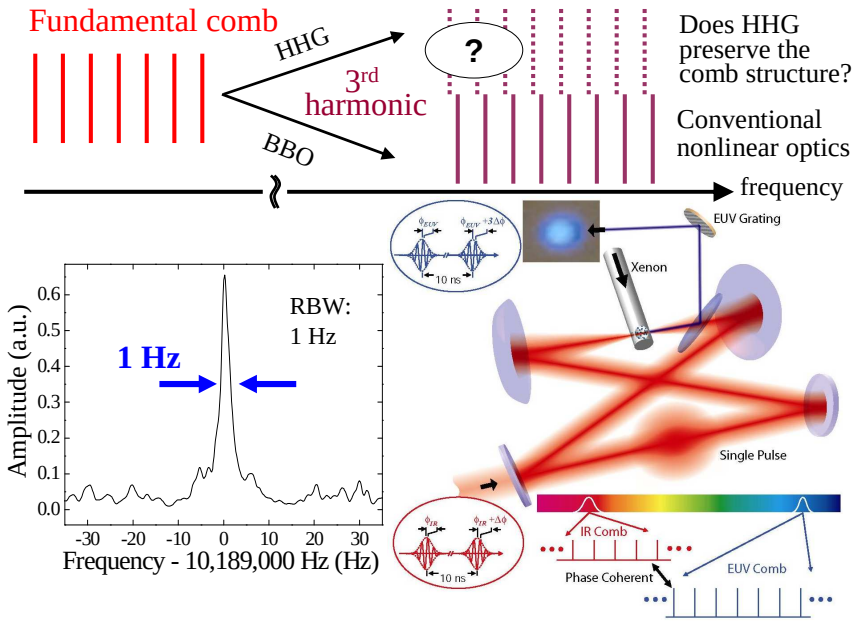

Figure 3. (a) Schematic setup for coherent heterodyne detection between HHG in Xe gas and bound optical nonlinearities in a BBO crystal. (b) Measurement of the optical beat signal between the two separately generated 3rd harmonics, indicating a coherent linewidth of 1 Hz, limited by the analyzer's resolution bandwidth. (c) Schematic setup of intracavity high-harmonic generation. The incident pulse train is stabilized to a high finesse cavity, enhancing pulse energy nearly three orders of magnitude while maintaining a high repetition frequency. A gas target at the cavity focus enables phase-coherent high-harmonic generation, resulting in a phase-stable frequency comb in the XUV spectral region. The photo inset shows the actual spatial mode profile of the 3rd harmonic coupled out of the cavity.

through the HHG process (Fig. 3). Two sets of the frequency combs at 266 nm that represent the third harmonic of the fundamental IR comb are then brought together in a Mach-Zehnder interferometer geometry for beat detection, after these two separate pulse trains are temporally overlapped. A 90 MHz acousto-optic modulator is inserted in one of the interferometer arms so that the beat detection is shifted to a convenient non-zero frequency. Pairs of corresponding comb components from each spectrum produce a coherent optical beat detected by a photomultiplier. The radio frequency spectrum of the beat note shows the clear presence of the comb structure in the UV (Fig. 3). The resolution bandwidth-limited 1 Hz beat signal demonstrates that the full spectral resolution and temporal coher-

ence of the original near-IR comb has been faithfully transferred to higher harmonics in this process.

Acknowledgments

We gratefully acknowledge the contributions of T. Loftus, R. Santra, E. Arimondo, and C. Greene on Sr experiments, D. Felinto, F. Cruz, and J. Lawall on united time-frequency spectroscopy, S. Diddams, T. Parker, and L. Hollberg for help in the delivery of NIST Cs fountain-calibrated maser signals to JILA, and J. Hall for the encouragement and support of our work.

References

1. T. H. Loftus *et al.*, *Phys. Rev. Lett.* **93**, 073003 (2004); *ibid. Phys. Rev. A* **70**, 063413 (2004).
2. X. Xu *et al.*, *Phys. Rev. Lett.* **90**, 193002 (2003).
3. T. Ido *et al.*, *Phys. Rev. Lett.* **94**, 153001 (2005).
4. A.D. Ludlow *et al.*, arXiv:physics/0508041 (2005).
5. R. Santra *et al.*, *Phys. Rev. Lett.* **94**, 173002 (2005).
6. M. Notcutt *et al.*, *Opt. Lett.* **30**, 1815 (2005).
7. A. Marian *et al.*, *Science* **306**, 2063 (2004).
8. A. Marian *et al.*, *Phys. Rev. Lett.* **95**, 023001 (2005).
9. R.J. Jones *et al.*, *Phys. Rev. Lett.* **94**, 193201 (2005).
10. C. Gohle *et al.*, *Nature* **436**, 234 (2005).
11. S. Cavalieri *et al.*, *Phys. Rev. Lett.*, **89**, 133002 (2002).
12. S. Witte *et al.*, *Science*, **307**, 400 (2005).
13. C. W. Oates, E. A. Curtis, and L. Hollberg, *Opt. Lett.* **25** 1603 (2000).
14. U. Sterr *et al.*, *Comptes Rendus Physique* **5**, 845 (2004).
15. M. Takamoto *et al.*, *Nature* **435**, 321 (2005).
16. S. G. Porsev and A. Derevianko, *Phys. Rev. A* **69**, 042506 (2004).
17. R. Santra *et al.*, *Phys. Rev. A* **69**, 042510 (2004).
18. T. Ido and H. Katori, *Phys. Rev. Lett.* **91**, 053001 (2003).
19. H. Katori, T. Ido, and M. Kuwata-Gonokami, *J. Phys. Soc. Japan* **68**, 2479 (1999).
20. H. J. Kimble *et al.*, *Proceeings of ICOLS'99 (XIV Inter. Conf. Laser Spectroscopy)* Eds. R. Blatt, J. Eschner, D. Leibfried, F. Schmidt-Kaler, World Scientific, Singapore 1999, pp. 80.
21. I. Courtillot *et al.*, *Phys. Rev. A* **68**, 030501(R) (2003).
22. T. Hong *et al.*, physics/0504216 (2005).
23. C. W. Hoyt *et al.*, physics/0503240 (2005).
24. J. Ye *et al.*, *J. Opt. Soc. Am. B* **20**, 1459 (2003).
25. D. Felinto, L. H. Acioli, and S. S. Vianna, *Phys. Rev. A* **70**, 043403 (2004).
26. R.J. Jones and J. Ye, *Opt. Lett.* **27**, 1848 (2002).
27. M.J. Thorpe *et al.*, *Opt. Express* **13**, 882 (2005).
28. R.J. Jones, I. Thomann, and J. Ye, *Phys. Rev. A* **69**, 051803(R) (2004).